# Wavefront Measurement for Laser-Guiding Diagnostic

S. Shiraishi[*,†], A. J. Gonsalves[*], C. Lin[*], K. Nakamura[*], J. Osterhoff[*], T. Sokollik[*], J. van Tilborg[*], C. G. R. Geddes[*], C. B. Schroeder[*], Cs. Tóth[*], E. Esarey[*] and W. P. Leemans[*]

*LOASIS Program, Lawrence Berkeley National Laboratory, Berkeley, California 94720, USA
†University of Chicago, Chicago, Illinois 60637, USA

**Abstract.** The wavefront of a short laser pulse after interaction in a laser-plasma accelerator (LPA) was measured to diagnose laser-guiding quality. Experiments were performed on a 100 TW class laser at the LOASIS facility of LBNL using a hydrogen-filled capillary discharge waveguide. Laser-guiding with a pre-formed plasma channel allows the laser pulse to propagate over many Rayleigh lengths at high intensity and is crucial to accelerate electrons to the highest possible energy. Efficient coupling of laser energy into the plasma is realized when the laser and the channel satisfy a matched guiding condition, in which the wavefront remains flat within the channel. Using a wavefront sensor, the laser-guiding quality was diagnosed based on the wavefront of the laser pulse exiting the plasma channel. This wavefront diagnostic will contribute to achieving controlled, matched guiding in future experiments.

## INTRODUCTION

Laser-plasma accelerators (LPAs) [1] have demonstrated accelerating gradients thousands of times greater than those in conventional accelerators. Employing a hydrogen-filled capillary discharge waveguide, a high-quality GeV electron beam has been produced within a few centimeters, demonstrating that LPAs have great potential for reducing accelerator size and cost [2, 3]. In this scheme, the radiation pressure of a high intensity laser pulse drives a wake in a plasma, creating ultra high longitudinal electric fields in which electrons can be accelerated. One limitation to the energy gain in LPAs is the length over which the laser pulse remains focused. Using a capillary waveguide to create a preformed plasma channel, laser pulses have been guided over many Rayleigh lengths, minimizing diffraction and accelerating electrons to a higher energy.

Experiments performed so far utilize a single laser that drives the wakefield for acceleration, and if the laser is guided, energy gain is limited by depletion. For applications such as high energy colliders, laser-plasma accelerator designs will rely on sequencing multiple acceleration stages, each driven by its own laser, to achieve collision energy [4]. Critical components in the planned staging experiment at LOASIS to demonstrate coupling between two stages include the injection of electrons, a plasma mirror to couple the stages, and electron acceleration. Electrons are injected only within the 1$^{st}$ stage, and the purpose of the 2$^{nd}$ stage is to produce efficient acceleration. In the 2$^{nd}$ stage, we drive the plasma wakefield in the quasi-linear regime to avoid electron trapping. Simulation studies on a quasi-linear stage design show matched guiding is critical to successful acceleration [5]. Examples of guiding diagnostics that have been used so far include spot size measurements at the output of the capillary and channel property measurements using laser centroid oscillations [6, 7]. However, spot size measurements are sensitive to the mode quality of the probe laser pulse. Moreover, neither method is sufficient to measuring the effect of self-focusing.

In this paper, we report on a diagnostic based on wavefront measurements that provides focusing and defocusing information. The wavefront measurement is less sensitive to the laser mode, provides information on self-focusing, and simplifies evaluation of whether the guiding is matched or mismatched. When the laser does not exit the capillary at focus, the wavefront measurement can diagnose the guiding as mismatched in a single shot. When the laser exits the capillary at focus, the wavefront data can be analyzed along with spot size measurements and channel parameter scans to distinguish the matched and mismatched guiding.

The paper is organized as follows. Basic theory of laser propagation in a plasma channel in a linear regime is discussed to illustrate the concept of the wavefront diagnostic. Then, the experimental setup at LOASIS facility is described along with an explanation of how the wavefront measurements are used. Analysis of experimental data are

presented in the results section followed by a concluding summary.

## LOW POWER LASER-GUIDING IN A PLASMA CHANNEL

Understanding the evolution of a laser pulse in a plasma channel indicates the need for laser-guiding diagnostics. In capillary waveguides, the plasma channel has a parabolic plasma density profile in the transverse plane, $n(r) = n_0 + \Delta n r^2 / r_m^2$, where $n_0$ is the on-axis density [8], and $\Delta n$ is the channel depth at a matched spot size, $r_m$ [9]. Such channels can provide guiding for a laser pulse with a Gaussian intensity profile, $|a|^2 = (a_0 r_0 / r_s)^2 \exp(-2r^2/r_s^2)$, where $a_0$ is the normalized laser vector potential given by $a_0^2 \simeq 7.3 \times 10^{-19} \, (\lambda \, [um])^2 I_0 [\mathrm{Wcm}^{-2}]$, $r_0$ is the focal spot size, and $r_s$ is the spot size. At low power without self-focusing, with the laser focused at the channel entrance ($r_i = r_0$, $dr_s/dz = 0$), the laser pulse propagates in the channel according to [9]

$$r_s^2 = \frac{r_i^2}{2} \left[ 1 + \frac{r_m^4}{r_i^4} + \left(1 - \frac{r_m^4}{r_i^4}\right) \cos \frac{2\lambda z}{\pi r_m^2} \right], \tag{1}$$

where $\lambda$ is the laser wavelength, $r_i$ is the spot size at the entrance of channel, and $z$ is the propagation distance. Examples of matched and mismatched guiding are shown in Fig. 1 a) and b). The entrance of the capillary is set at $z = 0$, and the plasma channel is indicated in shaded purple. For matched guiding, $r_i = r_m = 22\mu m$, the laser retains its spot size as it propagates through the channel. Mismatched guiding is shown in Fig. 1 b), where the green dot-dashed line represents $r_m = 34$ $\mu m$ and the red solid line represents $r_m = 45$ $\mu m$. As a result of matched guiding, the laser focus would appear to have shifted downstream by the length of the channel. In the case of mismatched guiding, the focus shift may not match the length of the channel. In these examples, the effective focal shift compared to vacuum focus, $\Delta z$, is 13.5 mm for matched guiding shown in Fig. 1 a), and 13.5 mm or 27 mm for mismatched guiding shown in Fig. 1 b). In the experiment, we measured $\Delta z$ to diagnose the guiding quality with the wavefront sensor. When $\Delta z$ is not the channel length, guiding is mismatched. When $\Delta z$ is the channel length, there is an ambiguity of matched or mismatched guiding. In this case, gradually varying $r_m$ to track the laser envelope oscillation within the channel allows us to distinguish matched and mismatched case.
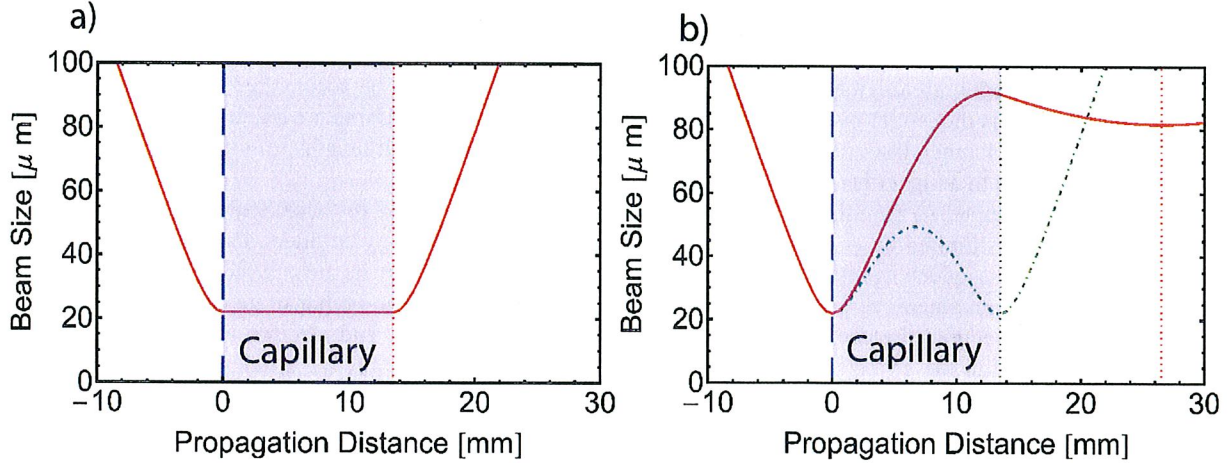


**FIGURE 1.** Calculated beam size as a function of propagation distance (solid lines). a) Matched guiding for the case of $r_i = r_m = 22$ $\mu m$ and b) mismatched guiding for the case of $r_i = 22$ $\mu m$, $r_m = 34$ $\mu m$ (green dot-dashed line) and $r_m = 45$ $\mu m$ (red solid line). Laser is focused at the entrance of plasma channel, $z = 0$. Dashed lines indicate the vacuum focus position and dotted lines indicate the effective focal position observing from downstream.

## EXPERIMENTAL SETUP

The laser-guiding experiment was performed using a 100 TW class Ti:sapphire laser system at the LOASIS facility. A schematic of the LPA experiment is shown in Fig. 2. An input laser was focused on the entrance of the hydrogen-filled capillary discharge waveguide [10, 11] by an off-axis parabolic mirror used at f/20. For a Gaussian transverse

intensity profile of $I = I_0 \exp\left(-2r^2/r_0^2\right)$, the average focal spot size was $r_0 \simeq 22\ \mu$m and the pulse duration was 45 fs in full width at half maximum. The experiment discussed in this paper was performed with low-intensity laser pulses ($\sim 10^{16}$ W/cm$^2$). While laser pulses with intensities greater than $10^{18}$ W/cm$^2$ are used for laser-plasma acceleration, working with low intensity laser pulses allowed us to investigate a regime where we could neglect non-linear effects such as self-focusing. This allowed us to concentrate closely on the effects of the plasma channel and laser-guiding.
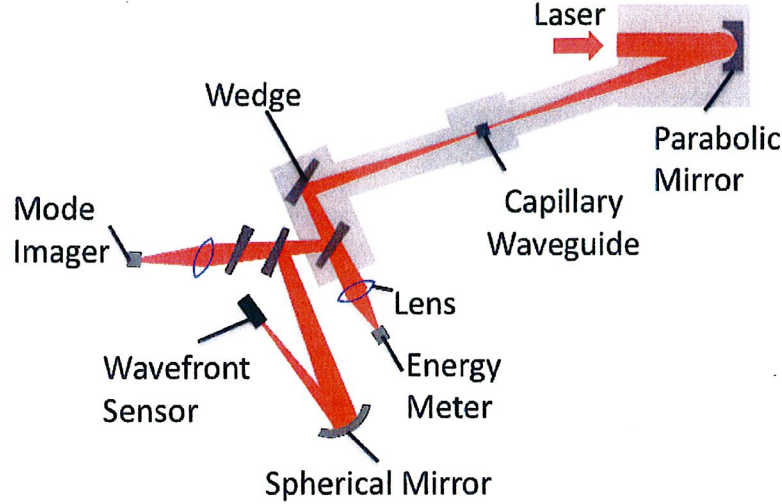


**FIGURE 2.** The experimental layout. Laser was focused onto capillary waveguide using a 2 m focal length off-axis parabolic mirror. Output laser pulse was attenuated with several wedged mirrors and weakly focused onto the wavefront sensor using a 1.5 m focal length spherical mirror. Laser energy and mode images were measured along with the wavefront.

The waveguide was laser-machined in sapphire plates, forming a 13.5 mm long by 250 $\mu$m diameter capillary. Hydrogen gas was introduced with a pressure of 100 Torr through a slot located at the end of the capillary. A high voltage discharge between electrodes placed at the ends of the capillary fully ionized the gas and formed a plasma channel. The plasma channel evolved from hydrodynamic motion in the capillary on the scale of tens of nanoseconds. Various channel conditions were formed by varying the time between the initiation of the discharge and arrival of the laser pulse. For this setup, electron density was $\sim 1 \times 10^{18}$ cm$^{-3}$ with a matched spot size of $\sim 45\ \mu$m based on a scaling law derived from the simulation in Ref. [12]. Since this particular capillary had only one gas slot, the plasma density within the capillary formed a gradient in the direction of the laser propagation. This feature made matched guiding impossible over the full length and made it difficult to predict the laser evolution in the channel.

Laser pulses exiting the plasma channel were imaged using a 1.5 m focal length spherical mirror to minimize chromatic aberration. The wavefront sensor used to measure the radius of curvature was located $\sim 5$ cm upstream of the image focus. The wavefront was measured using a lateral shearing interferometer, SID4, manufactured by Phasics [13, 14]. The SID4 wavefront sensor includes a 2D diffraction grating that splits the incident beam into four identical beams. These four beams form an interferogram pattern on the charge coupled device (CCD) of the camera. Deformations in the pattern are related to phase gradients. Using spectral analysis, SID4 retrieves a phase map for each laser pulse. An example of a measured interferogram and the retrieved phase map are shown in Fig. 3 a) and b). In our measurement, the dominant phase structure represents focusing from the spherical mirror. We compare the phase maps of the laser propagating in vacuum and in plasma. The deviation between the laser wavefronts in vacuum and in plasma describe how the laser propagates through the channel.

The measured wavefront was projected onto Zernike polynomials to extract the radius of curvature of each laser pulse. Zernike polynomials are orthogonal polynomials defined on a unit circle and are often used to describe aberrations [15]. Projecting onto Zernike polynomials also allowed us to separate beam tilts and other aberrations such as astigmatism and coma from focusing and defocusing effects. Using the Zernike defocus coefficient, $Z_{\text{def}}$, the

radius of curvature was calculated as

$$R_{\mathrm{c}} = \frac{A^2}{4\sqrt{3}Z_{\mathrm{def}}\lambda}, \qquad (2)$$

where $A$ was the radius of the wavefront map. Since Figure 3 c) shows the linear dependence between $R_{\mathrm{c}}$ and the sensor position for the range measured in the experiment, the measured $R_{\mathrm{c}}$ was taken to be the distance between the wavefront sensor and the image focus. With the measured $R_{\mathrm{c}}$, the focal position of the laser exiting the capillary waveguide, and
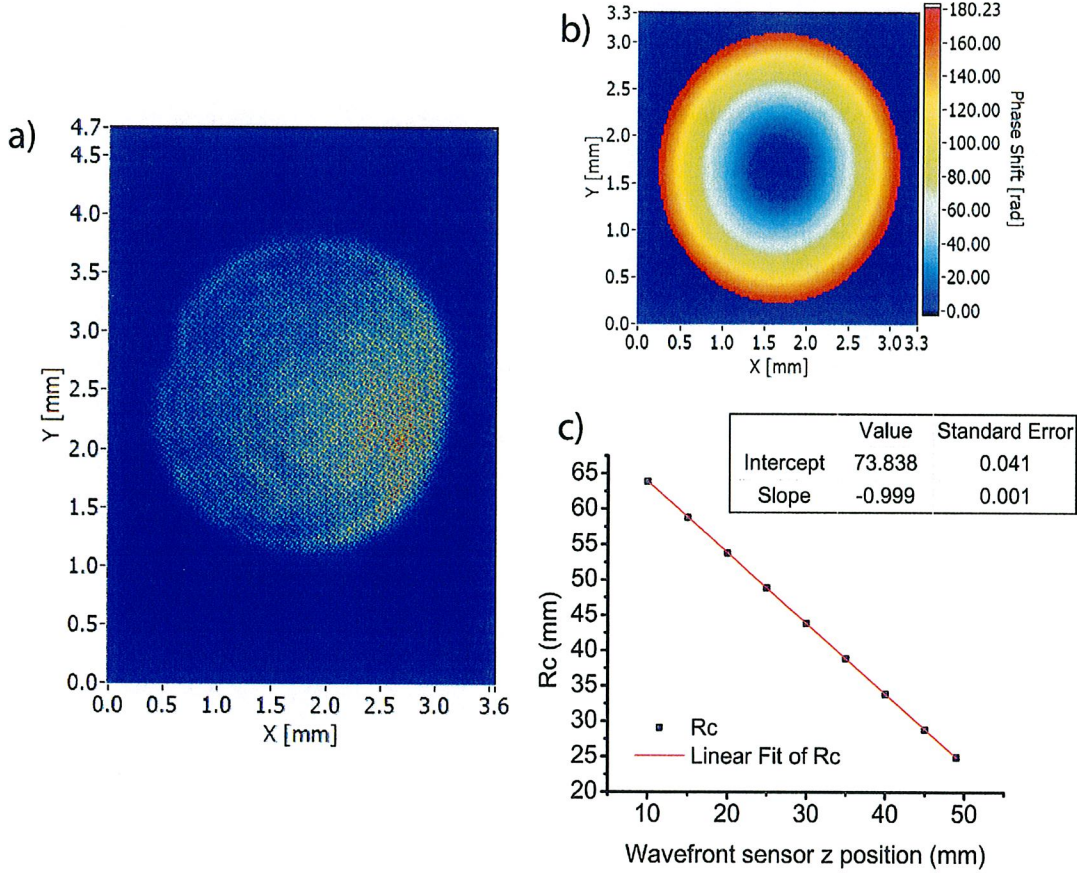


**FIGURE 3.** a) Interferogram taken by Phasics wavefront sensor for a laser pulse propagating without a capillary waveguide. b) Phase map retrieved from the interferogram. c) Measured $R_{\mathrm{c}}$ as a function of wavefront sensor position. Linear dependence between $R_{\mathrm{c}}$ and position is illustrated by the linear fit (red).

hence $\Delta z$, were calculated using a thin lens equation.

In addition, a photodiode was used to measure laser energy and a CCD camera was used to take a mode image for each pulse at the capillary exit plane allowing comparison with wavefront measurements. When the laser is guided efficiently, laser interaction with the capillary wall is minimized, yielding a cleaner output laser mode than that of a non-guided laser. Similarly, a well guided laser transmits a larger fraction of energy because it does not lose energy in the waveguide.

Finding the focal position of the laser using conventional diagnostics such as a mode imager requires multiple measurements at various image planes. Using the wavefront sensor, the focal position can be measured in a single shot. When the focal position is not at the exit of the capillary, laser guiding is mismatched. When the laser focus is at the exit of the capillary, a discharge timing scan that alters channel conditions can provide information about whether the guiding is matched or mismatched. Theoretically, the wavefront sensor can also retrieve beam size at the exit of the capillary based on a beam size at the wavefront sensor and the focal position. In short, the wavefront sensor is a tool to easily distinguish matched and mismatched guiding.

# RESULTS

The effective focal shift, $\Delta z$, calculated from the wavefront measurement as a function of discharge delay is shown in Fig. 4. The red curve is the discharge current. Since the density channel is a dynamic waveguide, shape and depth of the channel profile, and consequently $r_m$, depend on the discharge delay. Several stages in the evolution of the plasma can be identified.
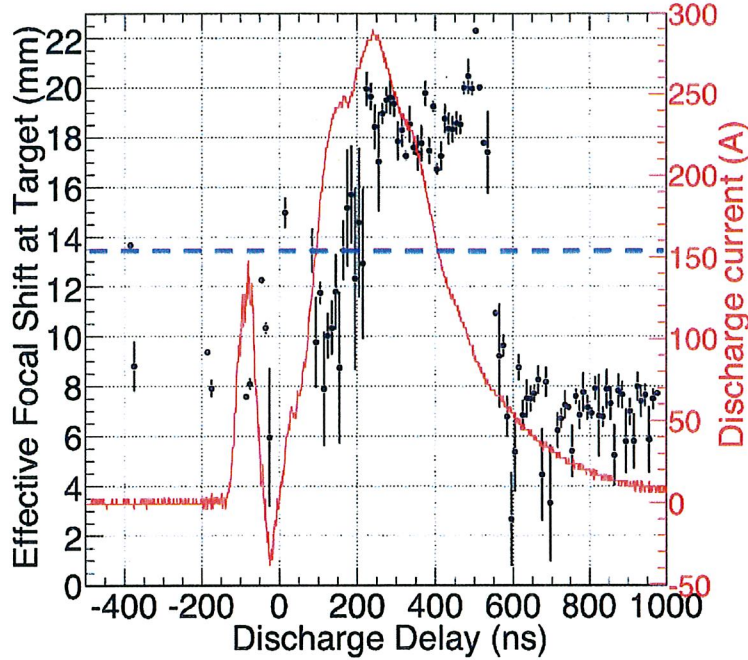


**FIGURE 4.** Low power laser-guiding data. Effective focal shift (black) and discharge current (red) as a function of discharge delay for 13.5 mm length capillary waveguide. The exit of the capillary is indicated with a blue dashed line. Hydrogen backing pressure into the capillary was 100 Torr.

The first stage occurs before full ionization of the plasma [16]. In this stage, the radial distribution of electron density is homogeneous and therefore no channel is present. When the plasma is fully ionized, the second stage begins. The discharge current leads to an increasing plasma temperature and the temperature gradient – hot on-axis and cold on the sapphire walls – redistributes the plasma to form a channel. Once the channel is fully formed, the plasma channel properties are approximately constant and independent of time [12, 16]. The parabolic plasma density profile remains until the hydrogen starts recombination.

In the experiment, the hydrogen was fully ionized around $\sim 100$ A and started to form a density channel. Until the delay at 200 ns, $\Delta z$ fluctuated suggesting that the channel was evolving. However, $\Delta z$ was stable at $\sim 19$ mm during the delay of 200 - 500 ns, suggesting a stable guiding regime. Around 500 ns, $\Delta z$ rapidly dropped to $\sim 8$ mm suggesting the channel was disappearing due to hydrogen recombination.

Laser mode images at the output of the capillary (Fig. 5) also verified guiding features of small spot sizes and high intensities for delays of 200 - 500 ns. The image on the left shows an intensity profile at 13.5 mm from the vacuum focus without a waveguide. The four sample images on the right are at the same location after the laser propagates through the capillary waveguide. Each image was taken at a different discharge delay indicated at the top. Intensity multiplication factors are shown on the top left corner of each image. The profile was the best for 200 - 500 ns, and examples are shown for 227 ns and 427 ns. These profiles have smaller spot sizes and higher intensities compared to those for 118 and 715 ns. Mode images suggest the laser was guided during 200 - 500 ns, which agrees with wavefront measurements.

Based on simulations, the matched spot size was calculated to be $\sim 45$ $\mu$m for this experiment. However, the measured $\Delta z$ ($\sim 19$ mm) was less than the analytical case (27 mm) for this $r_m$ shown in Fig. 1 b). The disagreement is likely due to the longitudinal density gradient across the capillary as discussed in the previous section. Since $r_m$ was a function of propagation distance in the experiment, predicting $\Delta z$ was difficult. Further analysis of the data is required

to fully understand the guiding conditions. Nevertheless, the wavefront measurements clearly indicate both guiding and not-guiding regimes and yields $\Delta z$ measurement. This experiment demonstrates a laser-guiding diagnostic can be based on wavefront measurements.
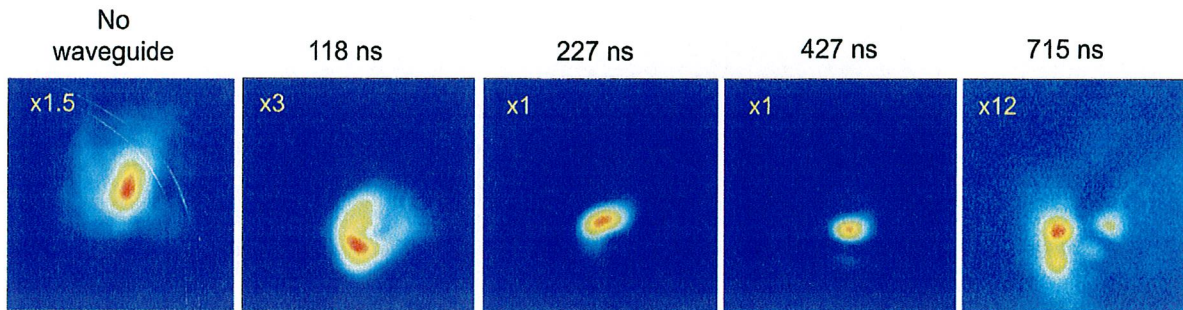
| No waveguide | 118 ns | 227 ns | 427 ns | 715 ns |
| --- | --- | --- | --- | --- |



**FIGURE 5.** Low power laser-guiding data. Mode images at various discharge timing. Intensity multiplication factors are shown on the upper left corner of each image.

## CONCLUSION

In summary, we have demonstrated a technique to determine laser-guiding quality based on a wavefront measurement. Since matched guiding is crucial for efficient electron acceleration, a reliable laser guiding diagnostic tool is important for LPA experiments, including those on the staging. The experiments described in this paper show that the guiding regime indicated by the wavefront measurement agrees with results from the mode imager. For a low power guiding experiment, we observe effective focal shifts ($\sim 19$ mm) that are much larger than the length of the capillary (13.5 mm), suggesting mismatched guiding. In the future, we will use this technique in high power experiments to study the effects of relativistic self-focusing on guiding. Ultimately, we plan to diagnose and control guiding with this method to achieve matched guiding in LPA stages.

## ACKNOWLEDGMENTS

## REFERENCES

1. E. Esarey, C. B. Schroeder, and W. P. Leemans, *Review of Modern Physics* **81**, 1229–1285 (2009).
2. W. P. Leemans, et al., *Nature Physics* **2**, 696 (2006).
3. K. Nakamura, et al., *Physics of Plasmas* **14**, 056708–8 (2007).
4. W. P. Leemans, and E. Esarey, *Physics Today* **62**, 44 (2000).
5. E. Cormier-Michel, et al., *AIP Conference Proceedings* **1086**, 297–302 (2009).
6. A. J. Gonsalves, et al., *Physics of Plasmas* **17**, 056706 (2010).
7. P. S. Antsiferov, M. R. Akdim, and H. T. van Dam, *Review of Scientific Instruments* **78**, 123107 (2007).
8. P. Sprangle, J. Krall, and E. Esarey, *Physical Review Letters* **73**, 3544 (1994).
9. E. Esarey, et al., *IEEE Journal of Quantum Electronics* **33**, 11 (1997).
10. D. J. Spence and S. M. Hooker, *Journal of the Optical Society of America B - Optical Physics* **17**, 1565 (2000).
11. A. J. Gonsalves, et al., *Physical Review Letters* **98**, 025002 (2007).
12. B. H. P. Broks, W. van Dijk, and J. J. A. M. van der Mullen, *Journal of Physics D: Applied Physics* **39**, 2377–2383 (2006).
13. Phasics (2010), URL http://www.phasics.fr.
14. S. Velghe, et al., *Optics Letters* **30**, 245 (2005).
15. M. Born and E. Wolf, *Principles of Optics*, Cambridge University Press, The Edinburgh Building, Cambridge CB2 2RU, UK, 1999, ISBN 0-521-64222-1.
16. N. A. Bobrova, et al., *Physical Review E* **65**, 016407 (2001).

# DISCLAIMER